Increasing Accuracy in Super-Resolution PIV

Theunissen R.[*], Stitou A.[+]; Riethmuller M.L.[*]
[*] Von Karman Institute for Fluid Dynamics
72, Chaussée de Waterloo
1640 Rhode-Saint-Genèse
BELGIUM

raf.theunissen@vki.ac.be; riethmuller@vki.ac.be

[+] Currently at University of Cambridge
Insect Flight Group - Micro Air Vehicle Project
Downing Street - Cambridge CB3 2EJ – UK

as703@hermes.cam.ac.uk

ABSTRACT

In the development of new measurement techniques, increasing the resolution has always been one of the main goals. For the moment, cross-correlation algorithms such as PIV, are limited by the size of the interrogation areas. Algorithms of hybrid PIV-PTV processing, so called Super Resolution methods, are about to be mature and have shown an increase in the spatial response. The present work is addressing the accuracy issue of such methods. An approach that correlates individual particle images is developed and it is referred as the IPC method. It aims at improving the efficiency compared to the classical approach using estimators of the successive particle locations. Examples of application in vortical flows are presented aiming at discussing the ability to characterize coherent structures. Ideal cases of vortices are simulated with synthetic images. This work presents also measurements of the flow field behind a backward facing step at low Re (Re_h=5000) performed in a low speed wind tunnel (U_0=3.75 m/s, h=2cm, expansion ratio=1.2). Vortical structures are extracted and results obtained from the two approaches (correlation PIV, hybrid PIV-PTV) are compared.

1.0 INTRODUCTION

Vortical turbulent structures are playing an important role in many industrial and aeronautical interests. As an example, the reduction in strength of wingtip vortices is currently investigated by many instances (Scarano *et al.*, 2002). This type of research requires a proper characterization of flow structures. Instantaneous whole field velocity measurements are valuable because they provide information that allows an alternative interpretation with respect to the classical Reynolds decomposition. The concept of coherent structures has been introduced and has turned out to be an interesting approach for investigating unsteady and turbulent flow fields (Hussein, 1986). Indeed a statistical analysis cannot explain the entire phenomenon and give only a limited view of the physics. Recently, different tools were developed aiming at characterizing these vortices, such as wavelet analysis (Schram and Riethmuller, 2001) and a pattern recognition method (Scarano, 2000) among others. These methods highlight the need of whole field measurement techniques.

Particle Image Velocimetry is such a whole field measurement technique. A thin laser sheet enlightens a section of the flow field, which is sufficiently seeded with tracers. A CCD camera then

Theunissen, R.; Stitou, A.; Riethmuller, M.L. (2005) Increasing Accuracy in Super-Resolution PIV. In *Recent Developments in Non-Intrusive Measurement Technology for Military Application on Model- and Full-Scale Vehicles* (pp. 2-1 – 2-18). Meeting Proceedings RTO-MP-AVT-124, Paper 2. Neuilly-sur-Seine, France: RTO. Available from: http://www.rto.nato.int/abstracts.asp.

Report Documentation Page

Form Approved
OMB No. 0704-0188

1. REPORT DATE	2. REPORT TYPE	3. DATES COVERED
01 APR 2005	**N/A**	**-**

4. TITLE AND SUBTITLE	5a. CONTRACT NUMBER
Increasing Accuracy in Super-Resolution PIV	5b. GRANT NUMBER
	5c. PROGRAM ELEMENT NUMBER
6. AUTHOR(S)	5d. PROJECT NUMBER
	5e. TASK NUMBER
	5f. WORK UNIT NUMBER
7. PERFORMING ORGANIZATION NAME(S) AND ADDRESS(ES) **Von Karman Institute for Fluid Dynamics 72, Chaussée de Waterloo 1640 Rhode-Saint-Genèse BELGIUM**	8. PERFORMING ORGANIZATION REPORT NUMBER
9. SPONSORING/MONITORING AGENCY NAME(S) AND ADDRESS(ES)	10. SPONSOR/MONITOR'S ACRONYM(S)
	11. SPONSOR/MONITOR'S REPORT NUMBER(S)

12. DISTRIBUTION/AVAILABILITY STATEMENT
Approved for public release, distribution unlimited

13. SUPPLEMENTARY NOTES
See also ADM202216.

14. ABSTRACT

15. SUBJECT TERMS

16. SECURITY CLASSIFICATION OF:			17. LIMITATION OF ABSTRACT	18. NUMBER OF PAGES	19a. NAME OF RESPONSIBLE PERSON
a. REPORT	b. ABSTRACT	c. THIS PAGE			
unclassified	**unclassified**	**unclassified**	**UU**	**18**	

records the reflections of these tracers. In general, two snapshots separated by time steps in the order of 1 to 1000μs, are divided into smaller rectangular windows, called correlation windows or interrogation areas. For each interrogation area, the intensities in both frames are cross-correlated from which an ensemble averaged displacement is obtained. Note that it is also possible to record two sequential snapshots onto one frame; double-exposure single frame (Rehm and Clemens, 1999). In that case displacements are obtained through auto-correlation. However, the focus of this article will lie on the first type of correlation as it is nowadays more common. An extensive literature survey can be made in which authors propose a range of improvements in the correlation algorithms to increase its accuracy. To name two, sub-pixel window offset and iterative window deformation (Scarano and Riethmuller, 1999) have shown to be the most rewarding and promising. In order for the correlation peak to be distinct from the surrounding noise peaks, a minimum number of image pairs must remain within the interrogation windows, typically about 10 particle pairs (Westerweel, 1997). These two operations increase the correlation signal by minimizing the number of particles which disappear from the interrogation area during the time step ‘Δt, due to large in-plane translations or velocity gradients and out-of-plane motion (Keane and Adrian 1990, Huang *et al.* 1993, Cowen and Monismith 1997).

The spatial resolution of the velocity measurements is a critical issue because many post-processing tools need that the flow structures are sufficiently sampled in order to identify them but also to characterize them correctly. For cross-correlation PIV, the spatial resolution is determined by the size of the interrogation windows (Wereley and Meinhart, 2001). Despite all progress, the spatial resolution is limited by the number of particle images captured in the interrogation areas (Keane and Adrian, 1990) and hence inversely proportional to the correlation window size (Scarano and Riethmuller, 2000). This restriction lead to the development of Particle Tracking Velocimetry, in which the displacement of individual particles is determined.

PTV processes start with identifying the particles. Pixels are classified as particles if their intensity lies above a certain threshold (Kiritsis 1989, Stitou and Riethmuller 2001, Cowen and Monismith 1997) or when the intensity distribution resembles a Gaussian shape (Takehara and Etoh, 1999). A crucial step in PTV is the correct pairing of particles between the frames. This caused that PTV was originally only suitable for flows with a low seeding density. Flow structures were hence poorly sampled. Keane *et al.* (1995) introduced the concept of Hybrid PIV-PTV algorithms or super-resolution PIV (SRPIV). A super-resolution algorithm has been developed at the VKI (Stitou and Riethmuller, 2001). The idea is that one first performs PIV on the recorded images. Using the obtained displacement field and taking into account only particles inside a certain search area (centered on the predicted position), one narrows down the number of possible partners and reduces the number of false measurements. As such, one maintains the typical PIV seeding and greatly enhances the spatial resolution (Figure 1).

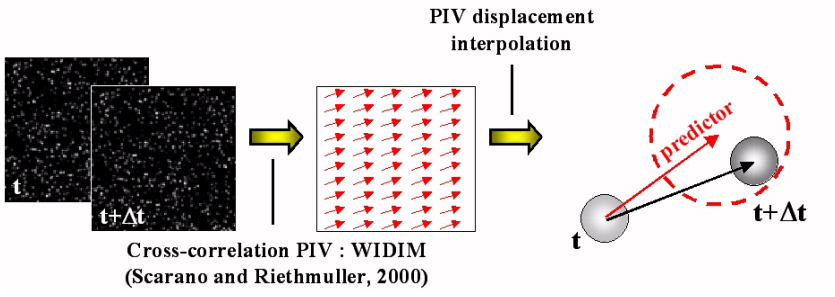

Figure 1: Principle of Hybrid PIV/PTV algorithms.

Both particle detection and pairing lie beyond the scope of this article. We address in the following discussion the accuracy issue supposing that the particle images are associated in a correct way. Logically, the displacement between two particles is represented by the vector connecting the particle centers. The simplest approach to find these centers seems to be the centroid method (Guezennec and

Kiritsis 1990, Udrea et al. 1996) in which the center of mass of the area illuminated by a particle spot is looked for. A variant consists in weighing every point with its intensity value. The method is very sensitive to the threshold that selects which pixels are accounted for. Since the particle image distribution can be modelized by a Gaussian curve (Adrian and Yao, 1983), three-points interpolation was applied (Wernet et al. 1993, Cowen and Monismith 1997, Zimmer 2001). Two-dimensional least square fitting has the advantages to use more points and is to be in theory less sensitive to the imaging noise (Udrea et al. 1996, Marxen et al. 2000, Takehara et al. 1999). These methods lead to a system of non-linear equations that need to be solved with an iterative numerical algorithm. The process is in general started using parameters from a simpler center estimator such as the centroid method. Marxen et al. (2000) reported in their work that this method presents an important drawback since it increases the computation time by a factor 100. Udrea et al. (1996) compared performances of different localization methods and concluded that particle center estimators not only show a random error due to noise but also a systematic error that is caused by the pixel discretization and depends on the sub-pixel position. Marxen et al. (2000) concluded that there is no major advantage of the least-square fitting over the 3-points Gaussian estimator but they considered isolated particles. Both works find an optimum size of around 4 pixels. In general the Gaussian interpolation performs well even though two-dimensional fitting could get some improvement especially when particle images overlap at intermediate and high concentration. Nevertheless, the PIV community agrees (Stanislas et al., 2003) on the fact that the accuracy of the measurement of PTV is presently lower than using correlation techniques. Indeed, this advantage is to be credited to the statistical nature of the correlation that operates on several tracers at the same moment in an interrogation area and, then, by incorporating the sources of errors, averages it. The sources of error are mainly due to the imperfect optics, to the digitization process and the inherent noise. Another source is the overlapping of individual particle image.

In this article an approach will be presented that correlates individual particles images and is referred to as the IPC method. It aims at improving the efficiency compared to the classical approach using the estimation of the successive particle locations.

2.0 PRINCIPLE OF INDIVIDUAL PARTICLE CORRELATION

The proposed method aims at overcoming the afore mentioned limitations of the centroid-search schemes and at improving the performances compared to the classical Gaussian fit method. The proposed feature is integrated at the end of the process of a hybrid PIV-PTV method. The particle images are identified on the two successive recordings. A first guess of the velocity map is evaluated using a correlation PIV method. Using this predictor field the particles are associated individually afterwards. The proposed idea in the present work is to correlate individual particle images instead of making the effort to localize them individually (Figure 2). The interest is then to take advantage of the averaging effect of the correlation operation. This approach will be referred as Individual Particle Correlation (IPC).

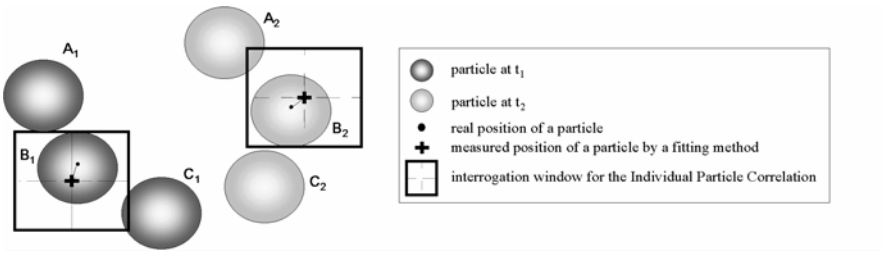

Figure 2: Principles of Individual Particle Correlation.

The processing is first initiated by the individual tracking of the tracers and then finalized with a statistical approach. The method is applied in the same fashion than any classical PIV iterative method.

Starting from an initial position estimated with a fitting approach, windows are correlated in a digital way and the relative displacement is determined. Then, the windows are shifted according to the previous partial measurement and the process is iterated several times. It is also possible to proceed in the same way as advanced PIV algorithms, by moving the two windows around a central point to obtain a second order accurate discretization of the flow field (Wereley and Meinhart, 2001). Since sub-pixel displacement of the windows is adopted, a re-sampling of the images is required. The scheme used is similar to the one used by Scarano and Riethmuller (2000). It consists on a development of Sinc functions (Hall, 1979).

Each window is centered around one complete particle instead of cuts of particle images as what is happening in the iterative correlation method as illustrated on Figure 3. In correlation PIV, more and more tracers are lying on the border during the refinement of the interrogation areas. Therefore, when a gradient of velocity is encountered, the signal-to-noise ratio of the correlation decreases because, in this case, the particles on the border are likely to move out of the correlated templates and do not contribute positively. The reduction of the windows size is therefore limited. On the contrary, in the IPC approach the source of information is always centered inside the interrogation area.

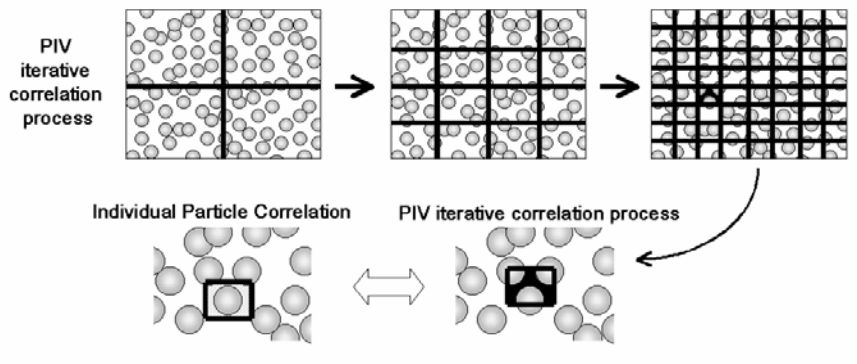

Figure 3: Comparison of the interrogation area obtained respectively with the IPC method and by a PIV iterative correlation process.

The correlation function is implemented using the following normalized formula:

$$C_{I_1,I_2}(\Delta x,\Delta y) = \frac{\sum\sum\left[I_1(x,y)-\mu_{I_1}(x,y)\right].\left[I_2(x+\Delta x,y+\Delta y)-\mu_{I_2}(x+\Delta x,y+\Delta y)\right]}{\sigma_{I_1}(x,y)\ .\ \sigma_{I_2}(x+\Delta x,y+\Delta y)} \quad (1)$$

The value μ_I and σ_I are respectively the mean and the standard deviation of the intensity of the templates. One advantage of using a normalized version of the correlation function is that it is possible to quantify the degree of matching between the two image samples. The function is computed in the spatial domain instead of using an FFT-based approach. Indeed, since the interrogation areas scale with the particle diameter, one has to deal with small windows. Therefore a direct correlation implementation offers a more efficient computational time.

In realistic situations, several sources of trouble can be listed: the imperfection and the pixelisation of the imaging system, the limited performances of image re-interpolator, the overlap of particle images. Example of successful measurements and non-successful ones are showed in Figure 4. Convergence occurs after less than 10 iterations (Figure 4a). It was observed that the iterative process of correlation does not converge in every situation (Figure 4b). The reason is the presence of other particle image in the neighbourhood. To prevent this situation, a check is performed at each iteration to ensure that the correction is at the sub-pixel level. If not, this process is abandoned and the Gaussian fitting is considered again.

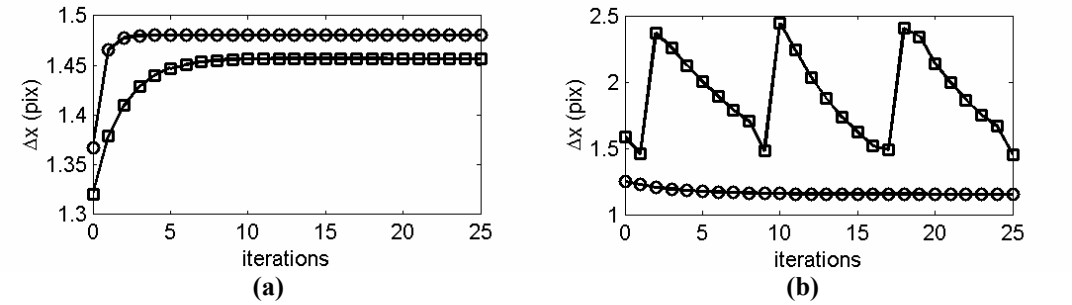

Figure 4: Implementation of the IPC method. (a) Converging case. (b) Diverging case.

3.0 ASSESSMENT OF INDIVIDUAL PARTICLE CORRELATION

3.1 Assessment of the Accuracy: Uniform Displacement Field

An assessment of the IPC method is proposed by means of synthetic images of reference velocity fields (Figure 6). Synthetic images of 200 by 200 pixels^2 were generated. Particles are uniformly displaced in both directions ($\Delta x=\Delta y=1.5$ pixels). This value was chosen because it is the one for which the highest random error is expected (Scarano and Riethmuller, 2000). Conservative conclusions can hence be made. The results are compared to the reference PIV method, named WIDIM. The dimension of the correlation area of the IPC method and WIDIM was varied and for each case a series of images was processed ensuring a sufficient number of samples to calculate the dispersion of the random error (around 1000 vectors).

The evolution of the RMS error of the displacement at a reference case with a concentration C_p=0.1part/pix^2 and source density N_S=0.9 is displayed in Figure 6a. The source density (Eq. 2) is related to the ratio between the spacing of the tracers λ_p and the particle image diameter D_p (Adrian and Yao, 1983). It is an indicator of the particle image overlap.

$$N_S = \left(\frac{C_{3D}\Delta z_o}{M_o^2}\right)\frac{\pi}{4}D_p^2 \propto C_p \cdot D_p^2 = \frac{number\ of\ particles}{image\ area}\cdot D_p^2 \propto \frac{D_p^2}{\lambda_p^2} \qquad (2)$$

A high value of N_S means a high concentration and vice versa. The SRPIV strategy starts by processing the images with standard PIV. After all window refinements, PIV stops at a correlation window of 16 by 16 pixels^2. After this, the PTV process kicks in and further refines the process to track individual particle images. The SPRIV strategy provides in those conditions an information spacing (vector spacing) of 4.3 pixels. The WIDIM performances seem not to be affected by the interrogation area dimension. Compared to the Gaussian fit, the IPC method performs better providing the window size around the particle is at least the size of the particle image itself. For a correlation area of 5 by 5 pixels^2, the improvement is of 40%. When increasing the window size, the error is decreasing till it reaches the same order of magnitude than the given PIV algorithm. This is a statistical effect since the number of pixels involved in the correlation is proportional with the square of the window size. Nevertheless, for this particle diameter (3 pixels) and the adopted windows size (5 pixels), the spatial resolution of the IPC (4.2 pixels) has still to be traded with the accuracy of the PIV.

A situation with a better resolved imaging sensor is simulated (Figure 5). One can also imagine using slightly defocused recordings to increase the size of the images of the tracers. The effect of the discretization of the image is presented in Figure 6. In the case of better sampling, the source density (N_S) and then the overlap factor is kept at the same level as the reference case even though the concentration expressed in particle/pixels^2 is lower. The Gaussian algorithm is improved because the discretization is

better. In the IPC process, the selected windows size is 7 pixels since the diameter of the particle images is 6 pixels. In that case, the accuracy of the IPC is comparable with the PIV one. The advantage is that the spatial resolution scales with the spacing of the particles (7.9 pixels) and not with the window size as with correlation PIV (each particle gets a vector). For a uniform displacement field, the dimension of the interrogation area of a correlation PIV algorithm can be highly reduced but for realistic flows containing gradients there is a limitation due to the in-plane loss of pairs (Keane and Adrian, 1993).

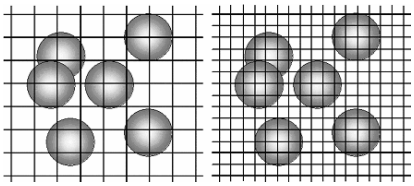

Figure 5: Effect of the image sampling $D_{p,1}<D_{p,2}$ - $C_{p,1}>C_{p,2}$ - $(\lambda_p/D_p)_1=(\lambda_p/D_p)_2$.

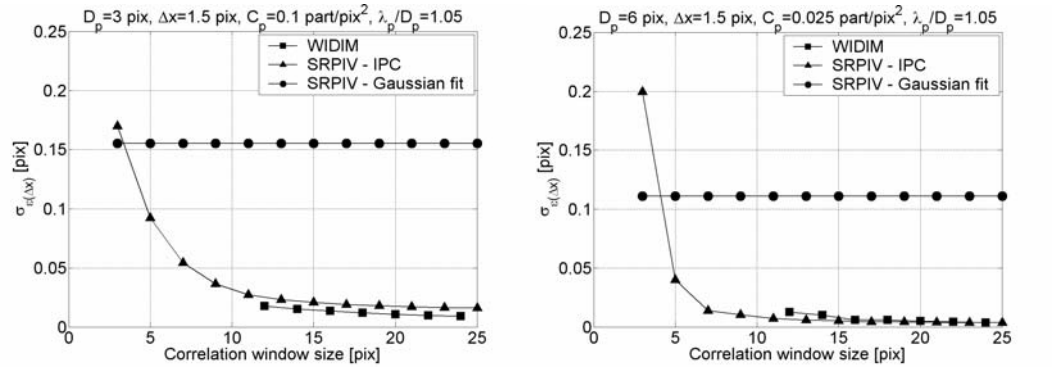

(a) **(b)**

Figure 6: RMS error obtained with the IPC method, the Gaussian fit and correlation PIV for different window-sizes (a) Reference case (b) Effect of better image sampling.

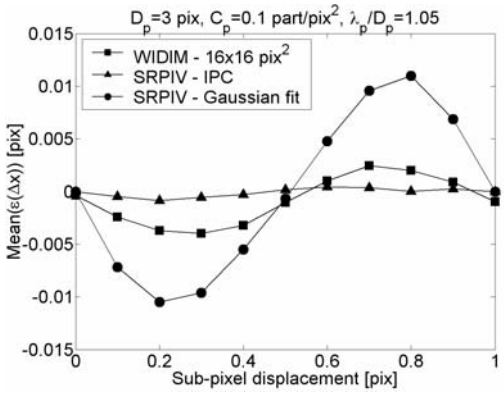

Figure 7: Systematic error in function of the applied sub-pixel displacement.

The characterization of the performances in term of systematic error is also performed by means of synthetic images. A database of images with uniform displacement of several amplitudes is constituted and processed. 16 by 16 pixels^2 windows size where considered for WIDIM as processing parameter for a reference. Figure 6 shows that the results are not in this case significantly influenced by the windows size. It is also reasonable parameters for a real processing. The mean of the measurement error in function of the sub-pixel part of the applied displacement is displayed on Figure 7. The pixelization introduces a periodical behaviour of the error with a periodicity of 1 pixel. This periodical behaviour is responsible for

the so-called pixel-locking. Looking to the sign of the systematic error, it is clear that the measurements are biased to the closest integer value. The SRPIV treatment with a Gaussian fit is giving the highest error. Switching to IPC mode removes it almost completely. It is also observed that this method shows an even lower error compared to the correlation PIV algorithm.

3.2 Assessment of the Spatial Response: Sinusoidal Displacement Field

The processing of a one-dimensional sinusoidal displacement field is an appropriate test case to examine the spatial response. The equations of the field are:

$$\begin{cases} \Delta x = A_0 . \sin\left(\frac{2\Pi}{\lambda_0} . y\right) \\ \Delta y = 0 \end{cases} \quad (3)$$

The amplitude A_0 is set to 2 pixels and the wavelength λ_0 is varied from 10 pixels to 100 pixels. The large wavelength corresponds to a low spatial frequency. The generated synthetic images are processed using the SRPIV strategy combined with the Gaussian fit approach and the IPC method. A structured vector field is obtained by using the AGW method (Agui and Jimenez, 1987) to redistribute the data. Results are compared to the reference PIV algorithm WIDIM (Scarano and Riethmuller, 2000). Interrogation areas of 12 by 12 pixels are correlated with an overlap factor of 75%. This velocity field is also used as a predictor for the tracking process. As depicted in Figure 8, a sinusoidal function is then fitted with the measurements to define the measured amplitude A_m.

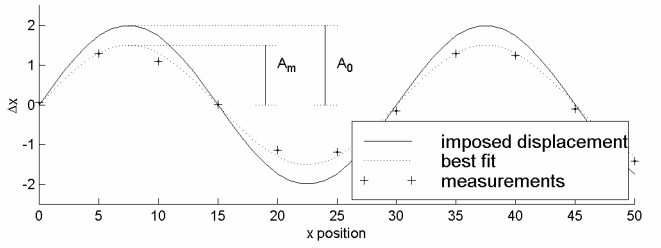

Figure 8: Methodology of the post-processing of the data.

The spatial modulation of the different techniques is defined as A_m/A_0. The plot on Figure 9 represents the modulation in function of the imposed wavelength λ_0. The diameter of the particle images is 3 pixels and several values of concentration are applied. The results do not show significant effect of the concentration in particles. For all processing method, the small wavelengths are more attenuated than the larger ones. It is observed that the two variants of the SRPIV method perform the same way.

Comparing to the correlation algorithm, two modes can be observed. Submitted to large wavelength, the response of SRPIV is better whereas at small wavelength the opposite behaviour is observed. The switch between these two modes happens at a wavelength of around 37.5 pixels. It occurs at the same value for the considered range of concentration. It is expected that SRPIV performs at least the same way as PIV. A bilinear scheme is used to interpolate the PIV velocity predictor towards the scattered particle positions and its effect is suspected. It is indeed expected that this interpolator is always under-estimating. Therefore the algorithm is looking for a particle match in the wrong region since the predicted position is not correct enough. This loss of particles pair is increased if one uses a coarser PIV predictor for high spatial frequencies. The effect the velocity predictor is examined on the Figure 10. The modulation of SRPIV is compared for two different PIV predictors. The first one uses window size of 12 by 12 pix^2 and 24 by 24 pix^2 for the second one. It is clear that, with the coarse velocity predictor, the modulation factor of the SRPIV method is lower than in the reference case.

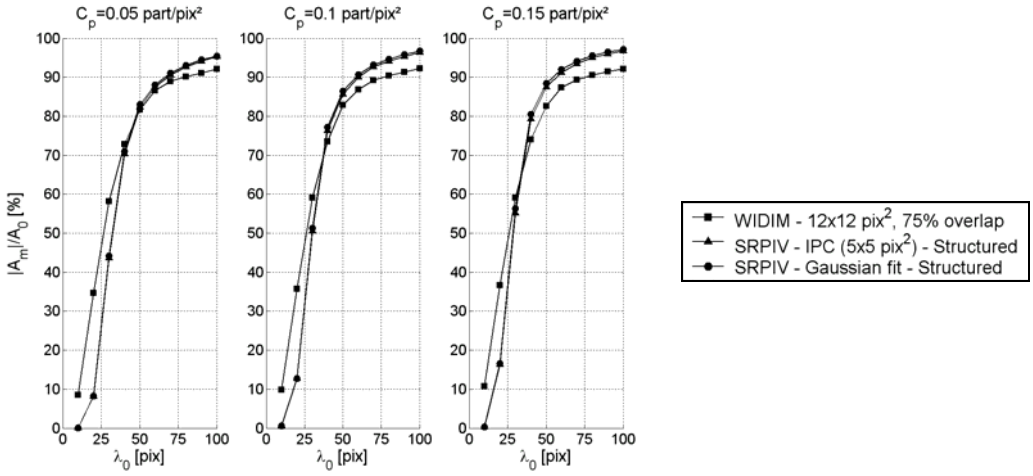

Figure 9: Modulation factor of an imposed sinusoidal velocity field (D_p=3 pixels).

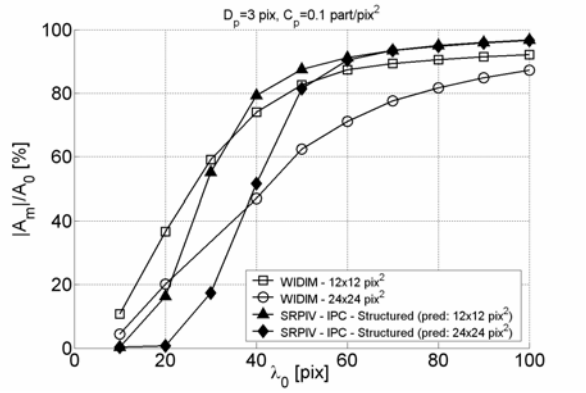

Figure 10: Effect of the velocity predictor on the modulation factor of the SRPIV method.

4.0 CHARACTERIZATION OF VORTICAL STRUCTURES

Vortical flows are present in numerous real flows of interest. They are of great industrial importance and specifically for the aerospace industry. Strong wingtip vortices behind commercial airplanes limit the time separation between aircrafts, which will without doubt lead to serious economic drawbacks. Reduction of this time interval requires a profound understanding of these wingtip vortices and hence accurate measurements. The vorticity is probably one of the most important parameters. The vortex shedding is also a dominant feature in combustion chambers. The characterization of the eddies would be valuable for the improvement of the design. More generally, turbulent flows are mainly dominated by the presence of organized coherent structures (Hussein, 1986).

We propose in this section to compare the ability of hybrid PIV-PTV to measure the characteristics of vortices and to compare it to the reference correlation PIV algorithm. Synthetic images of virtual vortices are valuable to assess the intrinsic performances.

4.1 Imposed Velocity Field

The influence of the particle image diameter, concentration, vortex radius and gradient is investigated. For each case, 100 images are used. The synthetic generated vortices were based on the Oseen-vortex model, which is given in polar coordinates in the equation below:

$$\begin{cases} u_r = 0 \\ u_\theta = \dfrac{\Gamma}{2\pi r}\left(1 - e^{-\frac{r^2}{\sigma_0^2}}\right) \\ u_z = 0 \end{cases} \quad (4)$$

From the relation above, the out-of-plane vorticity component and the gradient can be calculated:

$$\left.\begin{aligned} \omega_z &= \frac{1}{r}\frac{\partial r u_\theta}{\partial r} = \frac{\Gamma}{\pi\sigma_0^2} e^{-\frac{r^2}{\sigma_0^2}} \\ \nabla u &= \frac{\Gamma}{2\pi r^2} e^{-\frac{r^2}{\sigma_0^2}}\left(1 + 2\frac{r^2}{\sigma_0^2} - e^{\frac{r^2}{\sigma_0^2}}\right) \end{aligned}\right\} \quad (\omega_z)_{max} = (\omega_z)_{r=0} = \omega_0 = 2\cdot(\nabla u)_{max} = 2\cdot(\nabla u)_{r=0} = \frac{2\cdot\Gamma}{2\pi\sigma_0^2} \quad (5)$$

Note that the maximum vorticity equals two times the gradient in the center of the vortex. The gradient can be approximated as a linear function providing the radial distance is small enough.

4.2 Methodology

Different size of the interrogation areas are used during the PIV processing. Indeed, since the concentration of particles will be varied, the dimension of these windows has adapted at each case to keep a reasonable value of the correlation level. Concerning the SRPIV technique, the unstructured velocity field is redistributed toward a regular grid (Agui and Jimenez, 1987) in order to allow computing the vorticity map. The derivative of the velocity are computed using a central difference scheme:

$$\omega_z = \frac{\partial v}{\partial x} - \frac{\partial u}{\partial y} \approx \frac{v_{i+1,j} - v_{i-1,j}}{2h_x} - \frac{u_{i+1,j} - u_{i-1,j}}{2h_y} \quad (6)$$

To compare the ability to characterize vortical flows between the different image analysis approaches, a fitting is performed through the different data in order to extract the maximum measured vorticity (ω_m) and the dimensions (σ_m) of the imposed vortex as illustrated in Figure 11.

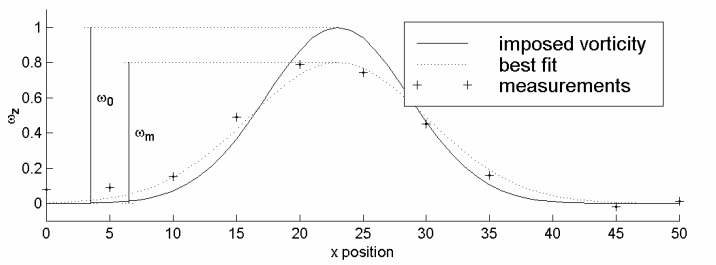

Figure 11: Characterization of vortices – data processing methodology.

4.3 Measured Velocity Field

The measured velocity field is discussed considering a reference case:

- Size of the particle image D_p=3pixels
- Seeding concentration C_p=0.1 part/pix^2
- Vortex with σ_0=50 pixels and ω_0=0.2 pix/pix with a maximum imposed displacement of 3.3 pixels

The influence of the variation of the parameters is addressed in the next section. Velocity maps are obtained and plotted in Figure 12. The circle represents the core of the imposed vortex. The correlation-based PIV is performed using windows of 12 by 12 pixels^2 overlapped by a factor of 75%, giving a vector every 3 pixels. The SRPIV provided a data every 4.4 pixels. Since the size of the particle spot is 3 pixels, an interrogation area of 5 by 5 pixels is adopted for the IPC method. All PTV fields are redistributed towards a regular grid of 5 pixels to compute derivatives. Although correlation based PIV returns more vectors, one must keep in mind that because of the large overlap, the vectors are not uncorrelated, which can lead to erroneous velocity/vorticity data.

A vorticity map is plotted in Figure 13 for all considered processing method. The higher scattering of the derivative quantity reveals the lower level of accuracy of PTV techniques respect to the correlation approach. Profiles are extracted and presented on Figure 14. All the velocity measurements are in agreement with the imposed vortex. The profiles of vorticity confirm the observation made on Figure 13 that the PTV measurements are dispersed around a trend that follows the real flow. It is to be noted that the random error level seems to be similar for the two variants of the PTV processing.

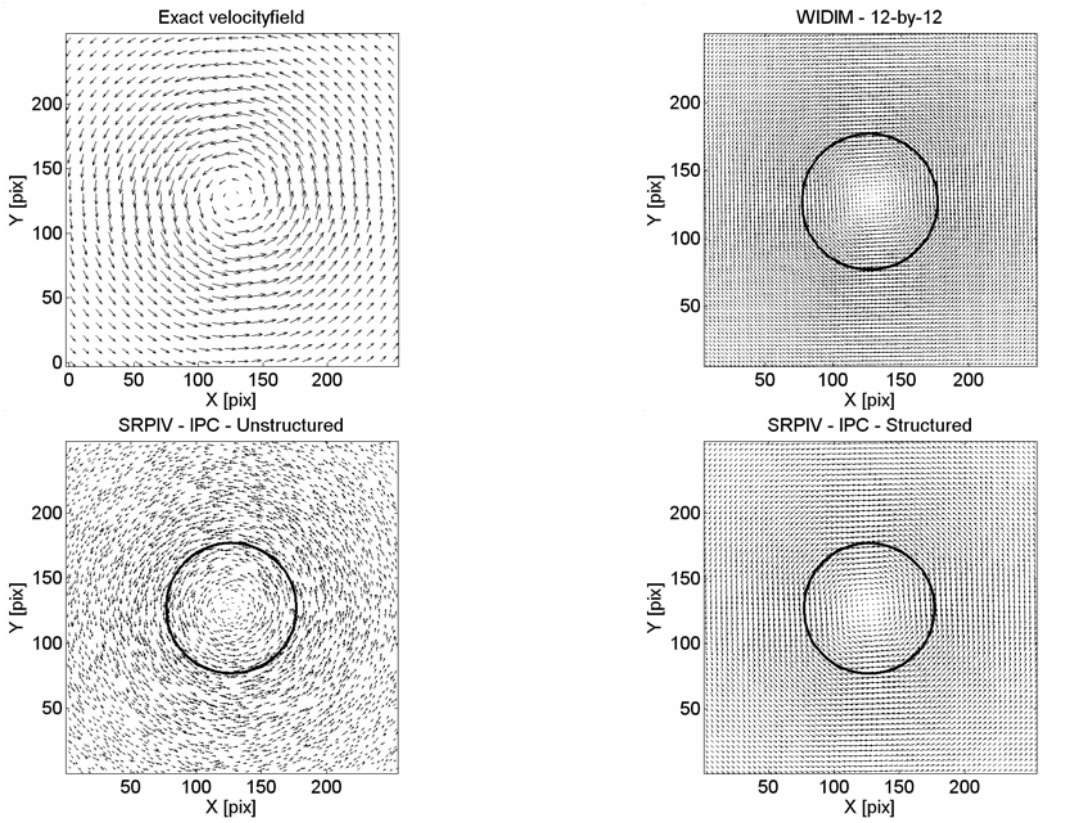

Figure 12: Velocity map obtained for a synthetic vortex.

The errors of the measurement using each method can be highlighted by establishing a cumulative histogram. The more the curve is on the left side of the graph the more accurate is the technique. Figure 15a demonstrates that the IPC method is able to provide more accurate measurement than the Gaussian fit approach in PTV. The advantage of correlation-based PIV is also confirmed. The situation is different when considering the redistribution of the unstructured PTV field towards a regular grid. The limited bandwidth of re-interpolator methods introduces some smoothing that can be valuable. The consequence is that the level of error is decreased as showed in Figure 15b. The disadvantage of the Gaussian fit in PTV is smeared out and the performances become similar to the IPC ones. In that case, it is also observed that the

IPC method performs in a very similar way to the PIV algorithm in term of accuracy, keeping the advantage of the higher spatial resolution of the PTV.

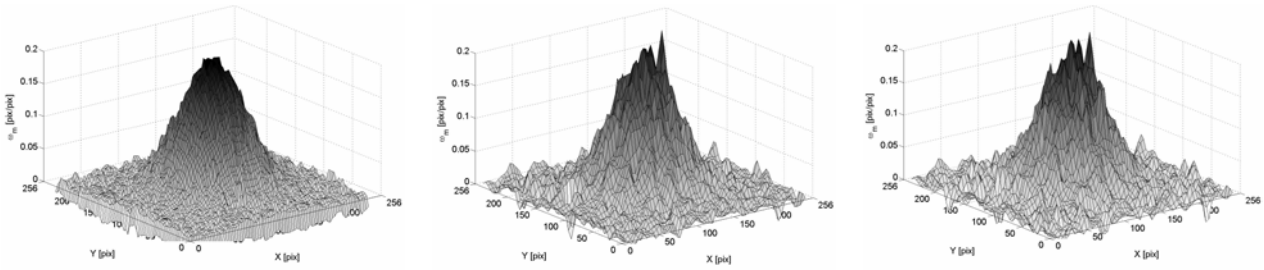

PIV – 12 by 12 pixels^2 (75% overlap) | SRPIV – IPC – 5 by 5 pixels^2 | SRPIV – Gaussian fit

Figure 13: Vorticity map for all considered processing approaches.

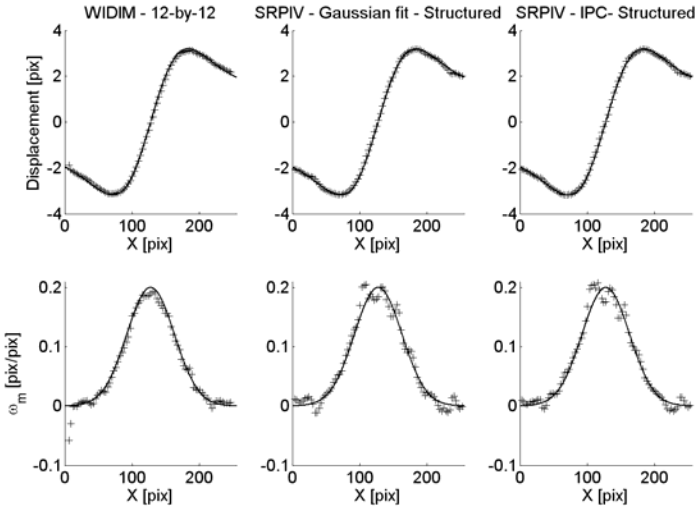

Figure 14: Velocity and vorticity profiles through the center of the vortex (solid lines represent the imposed vector, cross-hairs represent each considered technique).

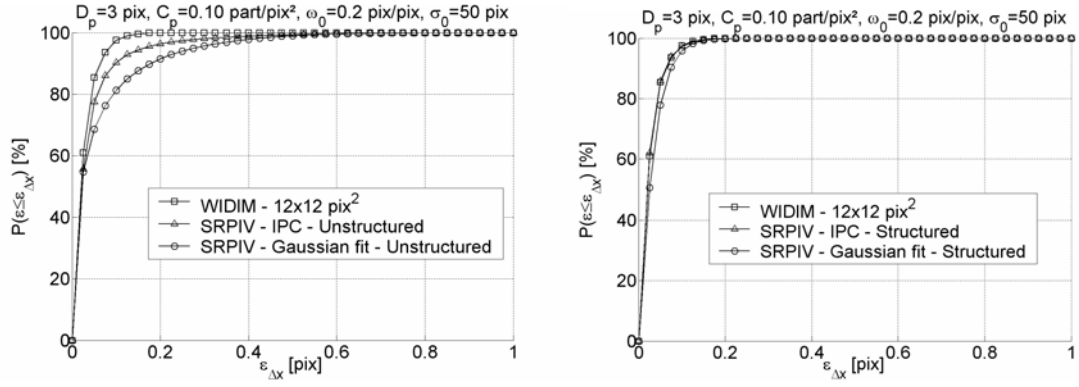

Figure 15: Cumulative histogram of error of measurement of the velocity.

4.4 Comparison in the Characterization of Vortices

The characterization of vortices by the different considered methods is presented in Figure 16 for the vorticity and in Figure 17 for the determination of the size of the imposed vortex. On each sub-graph, a

parameter is varied keeping the other ones constant. Table 1 summarizes the different cases. The successive considered variables are the imposed vorticity (ω_0), the concentration in seeding (C_p), the diameter of the particle spot (D_p) and the size of the imposed vortex (σ_0).

		a	b	c	d
ω_0	(pix/pix)	varied	0.2	0.2	0.2
C_p	(part.pix^2)	0.1	varied	0.1	0.1
D_p	(pix)	3	3	varied	3
σ_0	(pix)	50	50	50	varied

Table 1: Characterization of vortices – parameters of the synthetic images.

The modulation of the imposed vorticity (ω_m/ω_0) is investigated on the upper part of Figure 16. The imposed vorticity, the concentration and the diameter of particles size do not have a significant influence since the modulation remains almost constant for the considered range of parameters. The curve corresponding to the two variants of SRPIV method are almost superimposed. The performances are the same even though the IPC is intrinsically more accurate. It stresses again the fact that the redistribution step to a structured grid helps reducing the random error. As expected, going from a window size of 24 by 24 pixels^2 to 12 by 12 pixels^2 improves the spatial response of the processing by a correlation-based PIV algorithm. The SRPIV method presents an improvement respect to the PIV results that can reach 4% for the considering set of parameters. The value of the recovered vorticity is higher than 90%. This indicates a limited modulation of the vorticity. Nevertheless, when varying the size of the imposed vortex, the relative improvement of spatial response of the PTV is evolving. For instance, it ranges from 6% when σ_0 is 20 pixels to less than a percent when σ_0 is 80 pixels. More over, for a very small structure (σ_0 =20 pix), the recovered vorticity can drop to 91% for the SRPIV and 85% for the PIV.

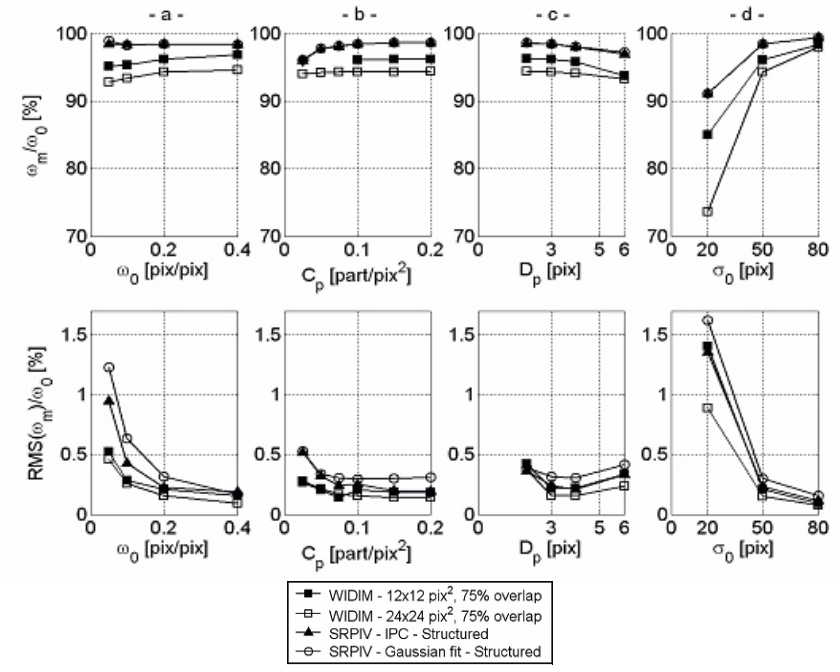

Figure 16: Characterization of vortices – measurement of the vorticity.

The relative error made on the measurement of the vorticity can be estimated from the value RMS(ω_m)/ω_0. This quantity is plotted on the lower part of Figure 16. In all cases, the error is less that 1.5% and the differences between the methods are not significant and are lower than a 0.5%. The PIV algorithm provides less scattered measurement since the plotted quantity is systematically lower. On

another hand the IPC method is slightly more reliable than the Gaussian fit approach. Neither the concentration in seeding of the particle diameter is affecting significantly the results. Nevertheless an optimum value between 3 and 4 pixels is recommended.

The assessment of the measurement of the vortex size is proposed in Figure 17. The measured size (σ_m) normalized by the size (σ_0) of the imposed vortex is plotted versus the considered parameters. In general, the measured vortex is systematically overestimated because (σ_m /σ_0) is always larger than 1. The imposed vorticity, the concentration and the diameter of particles size do not have a significant influence since the measured size remains almost constant for the considered range of parameters. PTV is overestimating by about 1% whereas PIV with an optimized interrogation window does by 2%. As expected, a larger interrogation area (24 by 24 pixels^2) is smoothing the field and one get a larger vortex. Concerning the error on the vortex diameter, the observations are strictly similar to the one made for the error of the measurement of the imposed vorticity. The results are proposed in the lower part of the Figure 17 for information.

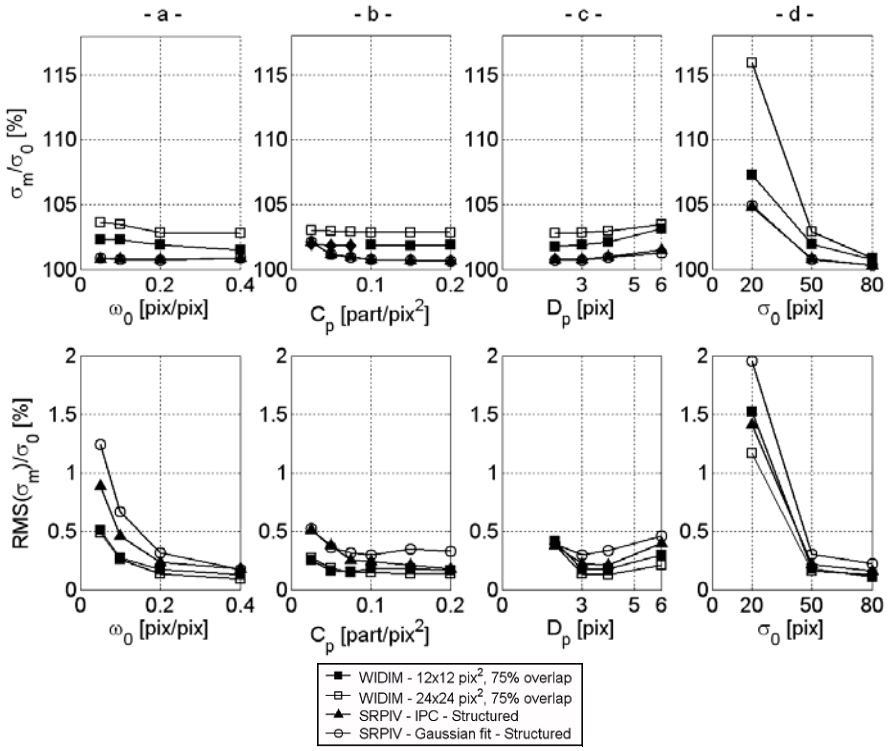

Figure 17: Characterization of vortices – measurement of the size of the core of the vortex.

5.0 APPLICATION TO THE TURBULENT FLOW PAST A BFS

The turbulent flow over a backward facing step (BFS) is a common test case adopted in experimental fluid dynamics as well in the CFD field. Although the geometry is simple and the location of the detachment point is stable, the flow field presents complex features. Measurements are taken in the plane of symmetry of the test section.

5.1 Experimental Conditions

A low speed wind tunnel with a cross-section of 20 by 20 cm^2 is operated with a centrifugal fan. The contraction ratio of the wind tunnel is 6. A splitter plate allows using half of the total section and the

flow is blown into a channel with a section of 10 by 20 cm^2. The backward facing step geometry is created by an expansion of the main channel. The step height h is 2 cm with an expansion ratio ER of 1.2. The flow conditions (U_o=3.75m/s,ν=1.5 10^{-5} m^2/s, h=2cm) at ambient temperature ensure a step-height-based Re_h around 5000. A turbulent boundary layer is trigged using a sand paper and it develops along the channel. The characteristics of the boundary layer are measured by Scarano and Riethmuller (1999). The boundary layer thickness δ is 1.2h with a maximum turbulence intensity level (Ti_{bl}) of 11% inside the boundary layer and 5% in the free stream (Ti_{fs}). A smoke generator is used to seed the flow. Information about the experimental conditions is summarized in Table 2 and illustrated on Figure 18.

The illumination source is a double pulsed Nd:Yag laser. It delivers 200 mJ at each pulse for a working frequency of 10 Hz. A classical arrangement is implemented to create a light sheet. The beam is first expanded with a cylindrical lens. A second spherical converging lens allows getting a plane with a thickness that is less than 1mm. Then the illumination plane is folded with a prism to reach the region of interest.

Geometry			Wind tunnel		Boundary layer			Flow conditions	
h	H	L	Section	U_0	δ	Ti_{bl}	Ti_{fs}	ER	Re_h
2	10	76	20 x 10	3.75	1.2	11%	0.5	1.2	5000
cm	cm	cm	cm^2	m/s	h	%	%	-	-

Table 2: BFS flow conditions

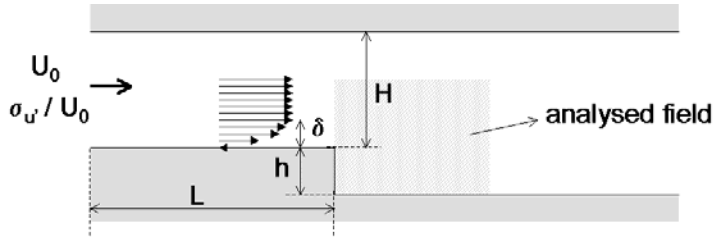

Figure 18: BFS configuration.

The analysed field is recorded by a cooled CCD camera (PCO Sensicam) with a quantization in 12-bits and with a resolution of 1280 by 1024 $pixels^2$. The region of interest covered 1280 by 640 $pixels^2$. The captured region spread over 4h downstream the step. For this configuration, the maximum frequency of acquisition is 5.71Hz. Since the laser is operated at 10 Hz, the camera is grabbing one pair of pulses over two at 5Hz. The maximum displacement of the particles on the images is set to 8 pixels and it is obtained with a laser pulse separation of 165µs.

5.2 Data Processing

Concerning the processing of the recordings by correlation, a compromise between spatial resolution and the number of validated vector is obtained by using a correlation window of 24x24 $pixels^2$ and an overlap of 50%. In that case, less than 1% of vectors are flagged as erroneous. The tracking method associated with the IPC approach is able to provide a vector every 4.6 pixels that are redistributed towards a regular grid with a pitch of 5 pixels.

Coherent structures are identified in the velocity field obtained by the PIV processing according to the wavelet analysis method proposed by Schram and Riethmuller (2001). In the identified regions, a Gaussian fit of the vorticity is performed with the same methodology than during the investigation of the synthetic images.

5.3 Characterization of the Identified Coherent Structures

Figure 19 presents the results in term of vorticity measurement. The histograms of measured vorticity are established for the two processing methods that are considered here. The vorticity is normalized with the step height and the free stream velocity. The most probable value of (ω_m.h/U_0) for the SRPIV is 6 whereas for the PIV it is 5. In that case, SRPIV is measuring higher value of the peak vorticity. Figure 20 presents the results in term of vortex sizing where, the measured size is normalized by the step height. These histograms show that the size of the vortices that is measured by PIV is larger. The most probable value for SRPIV is 0.1h and for PIV it is 0.115. These results are coherent with the conclusions made on the synthetic images analysis: the modulation of the SRPIV is lower than PIV and the overestimation of the vortex size done by SRPIV is lower than PIV. Nevertheless, more samples will be needed to have an accurate evaluation of the improvement.

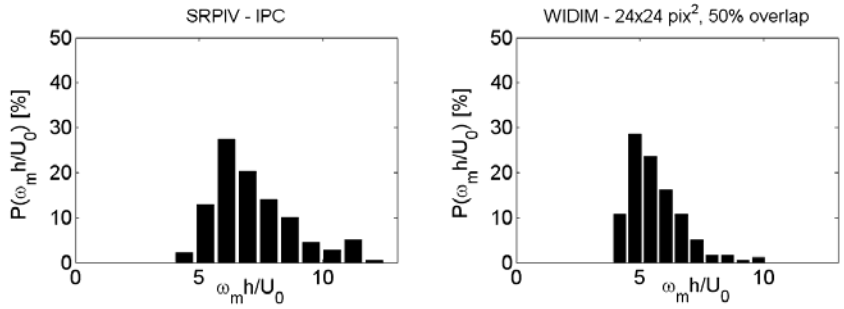

Figure 19: Application to the flow past a BFS – histogram of the normalized measured vorticity.

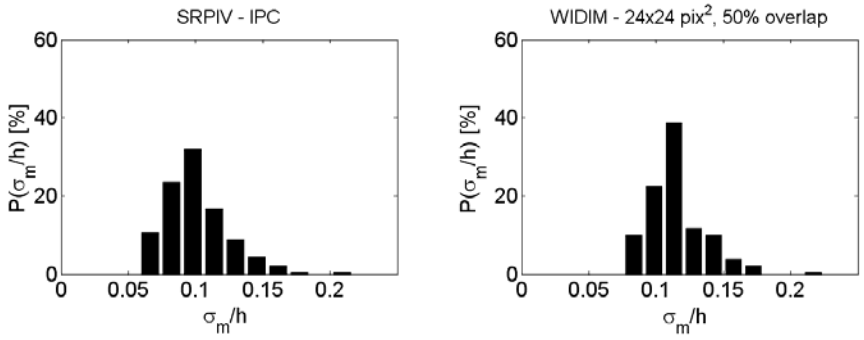

Figure 20: Application to the flow past a BFS – histogram of the normalized measured vortex-size.

6.0 CONCLUSIONS

It is always tempting to implement hybrid PIV-PTV method to improve the spatial resolution of correlation approaches. The accuracy of such method is addressed. A method based on the correlation of individual particle images (IPC) is proposed to improve the accuracy of classical Gaussian fit. A characterization was done on synthetic images. It showed that, for large particle images, the accuracy of the IPC is comparable with the PIV one. In that case, the advantage of PTV is that the spatial resolution scales with the spacing of the particles and not with the window size.

Synthetic images of a sinusoidal velocity field allowed evaluating the spatial response. An improvement of a few percents is obtained for the lower part of the spectrum. It was noticed that this behaviour is inverted from a certain imposed spatial frequency. The influence of the interpolator of the PIV predictor field is suspected. Indeed, this velocity field is interpolated towards the location of the tracer using a simple bilinear scheme. This issue deserves therefore further work in order to compare the potential benefit of higher order interpolator.

The application of hybrid PIV-PTV method to characterization of vortices is presented. The assessment on synthetic flow fields revealed that the effect of the redistribution of the scattered PTV vector map to a regular grid is not negligible. By using an AGW scheme, the error is decreased by smoothing the random error. It allows the SRPIV associated to the Gaussian fit method to reach an error level that is comparable to the IPC approach. In the considered cases, the IPC strategy showed to be able to reach the accuracy of a pure correlation algorithm. A general improvement of the modulation of the measured vorticity, that is 2% in average but can range up to 4%, is observed. Concerning the sizing of a given vortex, the improvement range from less than 1% and reaches 10% depending on the imposed structures size. The trend of these observations can be noticed when applying the techniques to the flow over a BFS. Nevertheless, the analysis of more samples will be needed to have an accurate evaluation of the improvement.

7.0 REFERENCES

[1] **Adrian R.J., Yao C.S.** (1983), Development of pulsed velocimetry for measurement of fluid flow, Proceedings of the *8th Symposium on turbulence*, Rolla (USA), pp.170-186.

[2] **Agui J.C., Jimenez J.** (1987), On the performance of particle tracking*, Journal of Fluid Mechanics, 185*, pp.447-468.

[3] **Cowen E.A., Monismith S.G.** (1997), A hybrid digital particle tracking velocimetry technique*, Experiments in Fluids*, *22*, pp.199 –211.

[4] **Guezennec Y.G., Kiritsis N.** (1990), Statistical investigation of errors in particle image velocimetry, *Experiments in Fluids*, *10*, pp.138 – 146.

[5] **Hall E.L.** (1979), Computer image processing and recognition, Ed. Academic Press, New York.

[6] **Huang H.T., Fielder H.E, Wang J.J., (1993)** , Limitation and improvement of PIV – Part I: Limitation of conventional techniques due to deformation of particle image patterns, *Experiments in Fluids*, *15*, pp.168-174.

[7] **Hussain K.M.F.** (1986), Coherent structures and turbulence*, Journal of Fluid Mechanics, 173*, pp.303.

[8] **Keane R.D., Adrian R.J.** (1990), Optimisation of particle image velocimeters, part 1: double pulsed systems, *Measurement Science Technology*, *1*, pp.1202-1215.

[9] **Keane R.D., Adrian R.J.** (1993), Theory of cross-correlation analysis of PIV images, *Flow Visualization and Image Analysis*, Kluwer Academic Publishers, Editor: Nieuwstadt F.T.M., pp.1-25.

[10] **Keane R.D., Adrian R.J., Zhang Y.,** (1995), Super-resolution particle imaging velocimetry, *Measurement Science Technology*, *6*, pp.1202-1215.

[11] **Kiritsis N.**, (1989), Statistical investigation of errors in Particle Image Velocimetry, *M.Sc. Thesis*, Ohio State University.

[12] **Marxen M., Sullivan P.E., Loewen M.R., Jähne B.** (2000), Comparison of Gaussian particle centre estimators and the achievable measurement density for particle tracking velocimetry, *Experiments in Fluids*, *29*, pp.145 – 153.

[13] **Rehm J.E., Clemens N.T.**, (1999), An improved method for enhancing the resolution of conventional double-exposure single-frame particle image velocimetry, *Experiments in Fluids, 26*, pp.497-504.

[14] **Scarano F., Benocci C., Riethmuller M.L.**, (1999), Pattern recognition analysis of the turbulent flow past a backward facing step, *Physics of Fluids*, Vol 11, Nr 12, pp 3808-3818.

[15] **Scarano F., Riethmuller M.L.** (1999), Iterative multigrid approach in PIV image processing with discrete window offset, *Experiments in Fluids*, *26-6*, 513-523.

[16] **Scarano F., Riethmuller M.L.** (2000), Advances in iterative multigrid PIV image processing, *Experiments in Fluids*, *29-S1*, 51-60.

[17] **Scarano F.,** (2002), Review article: Iterative image deformation methods in PIV, *Measurement Science and Technology*, *13,* pp.R1-R9.

[18] **Schram C., Riethmuller M.L.**, 2001, Vortex ring evolution in an impulsively started jet using digital PIV and continuous wavelet analysis, *Measurement Science and Technology*, Vol 12, Nr 9, pp 1413-1421.

[19] **Stanislas M., Okamoto K., Kähler C.** (2003), Main results of the First international PIV Challenge, submitted to *Measurement Science Technology.*

[20] **Stitou A., Riethmuller M.L.** (2001), Extension of PIV to super-resolution using PTV, *Measurement Science Technology, 12*, pp.1398-1403.

[21] **Stitou A., Theunissen R., Riethmuller M.L.** (2003), Advances in hybrid PIV-PTV techniques and application to vortical flows*, Proceedings of the EUROPIV2 Workshop on PIV*, Zaragoza (Spain), March 31-April 1.

[22] **Takehara K., Etoh T.** (1999), A study on particle identification in PTV- particle mask correlation method, J*ournal of Visualization*, *1*, 313 – 323.

[23] **Takehara K., Adrian R.J., Etoh G.T., Christensen K.T.** (2000), A Kalman tracker for super-resolution PIV, *Experiments in Fluids*, *29-S1*, 34 –41.

[24] **Udrea D.D., Bryanston-cross P.J., Lee W.K., Funes-Gallanzi M.** (1996), Two sub-pixel processing algorithms for high accuracy particle centre estimation in low seeding density particle image velocimetry, *Optics and Laser Technology*, *28-5*, 389-396.

[25] **Wereley S.T., Meinhart C.D.,** (2001), Second-order accurate particle image velocimetry, *Experiments in Fluids, 31*, pp.258-268.

[26] **Wernet M.P., Pline A.** (1993), Particle displacement tracking technique and Cramer-Rao lower bound error in centroid estimates from CCD imagery, *Experiments in Fluids*, *15*, 295 –307.

[27] **Westerweel J.**, (1997), Fundamentals of digital particle image velocimetry, *Measurement Science Technology, 8*, pp.1379-1392.

[28] **Zimmer L., Buchlin J.-M., Riethmuller M.L.** (1999), Particle Tracking Velocimetry and Sizing: Application to liquid sprays, *Proceedings of the International Workshop on Particle Image Velocimetry*, Santa-Barbara (USA), Sept. 16-18.